BMC Chemistry

RESEARCH

Open Access

Development and synthesis of DNA-based label-free electrochemical biosensor for detection of *Enterocytozoon bieneusi* using screen-printed gold electrode

Sara Nemati[1], Amir Sadeghi[2], Seyyed Mehdi Khoshfetrat[3], Hanieh Mohammad Rahimi[1], Kobra Omidfar[4,5*] and Hamed Mirjalali[1*]

Abstract

Microsporidia are a large group of obligate intracellular parasites. In this study, a label-free electrochemical genosensor was developed to detect *Enterocytozoon bieneusi* using specific probe and electrode substrate, Mxene-Ti3C2/AuNPs/PDA. A 5′ thiol-modified DNA probe, targeting 16S like ribosomal RNA (rRNA) gene of *E. bieneusi,* was designed. The Ti3C2-AuNPs-PDA nanocomposite was synthesized. The surface modification of the screen-printed gold electrodes (SPGE) was characterized by cyclic voltammetry (CV) and differential pulse voltammograms (DPVs) electrochemical methods. Scanning electron microscopy (SEM), transmission electron microscopy (TEM), fourier transform infrared spectroscopy (FTIR), and energy dispersive X-ray analysis (EDX or EDS) were employed to analyze the nanocomposites. The functional groups of Ti3C2/AuNPs/PDA nanocomposite were characterized using FT-IR spectroscopy. The SEM analysis revealed a layered accordion-like architecture of Ti3C2. The TEM image confirmed the deposition of composite on the substrates. The EDS mapping showed the elemental content of AuNPs, Ti3C2/AuNPs, and Ti3C2/AuNPs/PDA. A decrease in the peak of the current values was seen after adding *E. bieneusi* DNA, confirming formation of DNA—ssDNA complex. A limit of detection (LoD) of 0.06 pg mL-1 was obtained with a linear detection range 0.1–10 ^{4} pg mL-1. The integration of Ti3C2 and AuNPs not only facilitates the effective immobilization of DNA, but also improves the overall electron transfer kinetics. In addition, the developed genosensor demonstrated excellent sensitivity and selectivity with a low LoD of 0.06 pg mL-1.

Keywords Electrochemical biosensor, Label-free biosensor, Poly dopamine (PDA) nanofilms, MXene, *Enterocytozoon bieneusi*

*Correspondence:
Kobra Omidfar
omidfar@tums.ac.ir
Hamed Mirjalali
hamed_mirjalali@hotmail.com; hamedmirjalali@sbmu.ac.ir
Full list of author information is available at the end of the article

Introduction

Microsporidia are a group of obligate single-cell, spore-forming microorganisms containing over 220 genera and 1700 species [1, 2], among these at least 15 genera/species have been identified as human pathogens [3, 4]. Microsporidia have worldwide distribution, leading microsporidiosis in humans, particularly in immune-deficient individuals [5, 6]. The fecal–oral is the main transmission route for this group of pathogens, however, consumption of contaminated food and water, zoonotic infection, and inhalation of spores have been explained as potential transmission routes [7, 8]. Among human-infecting microsporidia, *Enterocytozoon bieneusi* is a well-described species in clinical settings [9, 10]. Recent data has classified microsporidia, particularly *E. bieneusi*, among emerging risk for food- and waterborne outbreaks [11]. Alongside with focuses on epidemiology of microsporidia, due to challenges in diagnosis, several methods have been developed to increase the accuracy of detection. Due to the need for a well-trained microscopist, false results are the main challenge in laboratories.

Due to the limitations of conventional parasitological methods, molecular approaches have been developed. Although molecular techniques may exhibit reduced sensitivity in light infections, they are primary tools for detection of *E. bieneusi*. To overcome limitations of the current molecular methods, new nucleic acid-based technologies such as Clustered Regularly Interspaced Short Palindromic Repeats (CRISPR) have been developed. However, several challenges including the cross-reactivity, sample complexity, and the presence of inhibitors can compromise the efficacy of molecular techniques, particularly in real samples. Therefore, developing of a high specific, user-friendly, and cost-effective system with rapid processing is essential [12, 13].

Biosensors represent a promising alternative for the screening and diagnosis of parasite infectious [14]. A typical biosensor system comprises three key components: (1) a bioreceptor (e.g., enzyme, antibody, cell, nucleic acid, aptamer) serving as the sensing element, (2) a transducer (e.g., semi-conducting material/nanomaterial), and (3) an electronic system for signal amplification [15]. Biosensors are broadly classified into electrochemical, electrical, optical, and mass based methods [16]. The electrochemical biosensors have been successfully developed for rapid detection of intestinal pathogenic microorganisms [17–19]. The incorporation of significant properties of electrochemical platforms with the high selectivity of nucleic acid approaches has resulted in development of DNA-based specific biosensing systems for detection of different agents [20]. Over the past decade, various signal amplification strategies have been employed to improve the sensitivity, signal-to-noise (S/N) ratio, and limit of detection (LoD) in electrochemical systems [21, 22]. Conducting polymers are widely used in designing and fabrication of biosensing systems [23–25]. Recently, poly dopamine (PDA) nanofilms have been generally utilized for the substrate modification [26, 27]. Due to the abundant catechol and amine groups, PDA facilitates immobilization of nanomaterials onto the surface of electrode, while introducing functional groups [28–30]. Furthermore, integrating two dimensional (2D) materials and nanoparticles with PDA has been suggested to improve the selectivity, sensitivity, and LoD of electrochemical biosensors [31].

Gold nanoparticles (AuNPs) have been widely utilized in electrochemical molecular diagnostics over the past two decades, due to their electrochemical characteristics [32–34]. Among various 2D materials, transition metal–carbon/nitrides, particularly Ti3C2 (MXene) nanosheets, have gained significant research interest owing to their excellent electrical conductivity, biocompatibility, thermal stability, as well as unique surface properties [35–37]. These outstanding features render MXene nanosheets highly suitable for developing sensitive electrochemical biosensors [38–40]. Moreover, inherent biodegradability and biocompatibility of MXene, make them promising candidates for clinical applications including drug delivery, tissue engineering, and biosensing systems, without eliciting adverse reactions [41–43]. Since the mussel-inspired adhesive protein properties [44], PDA has received extensive attention as multifunctional coating, due to its self-polymerization and spontaneous deposition on the surface of almost any materials under alkaline conditions to form a designable and flexible layer [45, 46]. Moreover, PDA exhibits versatile chemical reactivity during secondary reactions [45]. For instance, it can bind to metal ions and form a metal coating, due to the binding ability of catechol in PDA. This universal coating capability allows PDA functionalized diverse materials, such as polymers, metals, and ceramics. This polymerized layer, which is rich in catechol groups, allows easy immobilization of primary amine or thiol-based biomolecules through dipping [47, 48].

The current electrochemical biosensor operates on the principle that hybridization between target DNA and the immobilized probe impedes electron transfer, resulting in a measurable current decrease that correlates with DNA concentration, while maintain stable baseline current. The current study aimed to develop a label-free electrochemical DNA biosensor for specific detection of *E. bieneusi* DNA in clinical and environmental samples by immobilizing oligonucleotide probe as bioreceptor molecule, while Ti3C2/AuNPs/PDA nanocomposite film was

considered as a conducting substrate to improve the electron transfer reaction.

Experimental parts

Materials and instruments

Gold (III) chloride trihydrate ($HAuCl_4 \cdot 3H_2O$), dopamine hydrochloride (DA HCl: (HO) 2C6H3CH2CH2NH2. HCl, hydrochloric acid (HF), 2-mercaptoethanol (2-ME), sodium chloride (NaCl), potassium ferrocyanide ($K_4[Fe(CN)_6]$), and tris (2-carboxyethyl) phosphine) (TCEP), Tris (tris- (hydroxymethyl) aminomethane) (AlfaAesar) buffer (pH = 8.5, 7.0, 10.0), ammonium persulfate (AlfaAesar), sodium percarbonate potassium hexacyanoferrate- (III; 99%), and potassium hexacyanoferrate (II) (98.5 − 102%) were all purchased from Sigma-Aldrich, USA.

Monosodium phosphate (NaH_2PO_4), and disodium phosphate (Na_2HPO_4) were obtained from Merck (Darmstadt, Germany). All solutions were prepared using distilled deionized (DD) water (Purity, Prema, Taiwan). The screen-printed gold electrodes (SPGEs: 3.4 cm length × 1.0 cm width × 0.05 cm height) were purchased from Drop Sens (Spain) (www.dropsens.com/en/screen_printed_electrodes_pag). Electrochemical experiments were carried out using a potentiostat/galvanostat μStat 400, along with the DropView software package provided by DropSens, Spain (www.dropsens.com/en/potentiostats_pag/). Scanning electron microscope (SEM) images were acquired using a VEGA3-LMU (TESCAN, USA) (www.tescan.com/en-us/technology/sem/vega3). Field emission scanning electron microscopy (FE-SEM) imaging and energy dispersive spectroscopy (EDS) analyses were performed with a MIRA3-XMU FE-SEM (TESCAN, USA) (www.tescan.com/en-us/technology/sem/mira3).

Oligonucleotides

For designing a 5'thiol-modified DNA probe, a single primer, targeting small subunit (SSU) rRNA gene was employed to specifically amplify *E. bieneusi* [11]. The 5'thiol-modification was done to facilitate interaction between the probe with AuNPs on the substrate. To evaluate specificity of selected probe, a couple of mismatches were applied through the probe sequence. Probes were constructed by Bioneer corporation (South Korea) (Table 1).

Table 1 The designed probes and mismatch nucleotides in probe sequences

Probes	Sequences
Main	5'-(SH) GGTAATTTGGTCTCTGTGTG-3'
Mismach-1	5'-(SH) GGTAATTTG**T**TCTCTGTGTG –3'
Mismach-2	5'—(SH) GGTAATTTGGTCTCTGT**T**TG-3'
Mismach-3	5'-(SH) **T**GTAATTTGGTCTCTGTGTG-3'

The bold letter indicates mismatch

Synthesis of Ti3C2

The MXene was synthesized through etching bulk Ti3AlC2 [49], according to a modified version of a previously described method [50]. For this purpose, 1 gr of Ti3AlC2 powder was dissolved in 20 mL of 30% hydrofluoric acid (HF) with stirring at 25 °C for 12 h. Upon three times washing the product by deionized water (DI water), it was centrifuged at 8000 rpm. Then, the sample was dried at 65 °C in a vacuum oven [50].

Preparation of Ti3C2/AuNPs

Our prior study demonstrated that reducing tetrachloroauric acid ($HAuCl_4$) with trisodium citrate ($Na_3C_6H_5O_7$) yielded 20 nm AuNPs [51, 52]. In this regard, a solution of 1% $Na_3C_6H_5O_7$ was added to 100 ml of boiling $HAuCl_4$ (0.01% [w/v]), while it was constantly stirred. After ~8 min, when the solution had turned from yellow to wine red, it was cooled down to the 25°C. Concentrated sodium hydroxide (NaOH) was used to adjust the pH to 8.5, and then 0.01% (w/v) sodium azide (NaN_3) was added. Afterward, the resulting AuNPs solution was placed in a dark glass container and kept at 4°C for subsequent use. The AuNPs (0.3 mg/μL) were added into the Ti3C2 nano-sheets (1 mg/mL) by adding 5 mL of this solution to 1 mg of Ti3C2, while stirring at 25 °C [53]. Once the Ti3C2/AuNPs nanocomposites were synthesized, they were collected by centrifuging them, three times at 10,000 rpm with DI water, before being dried in a vacuum oven [54].

Synthesis of Ti3C2/AuNPs/PDA nanocomposite

First, the preparation of a 0.5 mg/mL DA solution was performed through dissolving 0.5 mg of DA hydrochloride powder in 1 mL of Tris buffer (10 mM, pH 8.5) [55]. Afterward, 40μL of the produced Ti3C2/AuNPs was added into the DA solution, and the mixture was stirred for 2 h at 25°C. Then, the mixture was centrifuged at 10,000 rpm for 10 min to remove any remaining impurities before being suspended in 1 mL of DI water. The reaction mixture was separated by centrifugation at 10,000 rpm for 10 min, followed by three washes in DI water and re-dispersing in 1 mL of DI water [56, 57]. To further confirmation of the presence of Ti3C2/AuNPs/PDA on synthetized nanocomposite, the SEM, transmission electron microscopy (TEM), fourier transform infrared spectroscopy (FTIR) and EDS analyses were carried out (Fig. 1).

Fig. 1 Synthesis procedures of Ti3C2/AuNPs/PDA nanocomposite. The process begins with the reduction of tetrachloroauric acid ($HAuCl_4$) using trisodium citrate ($Na_3C_6H5O_7$) to produce AuNPs

Brief overview of nanocomposite fabrication

The AuNPs (0.3 mg/μL) were added into the Ti3C2 nanosheets (1mg/mL) by adding 5 mL of this solution to 1 mg of Ti3C2, while stirring at 25°C. Then, 0.5 mg/mL of DA solution was prepared by dissolving 0.5 mg of DA-HCl powder in 1 mL of Tris buffer (10 mM, pH 8.5). After preparation of the working electrode, 10μL of the synthesized Ti3C2/AuNPs/PDA nanocomposite (25 μg/μL) was dropped on SPGEs and allowed to dry at 25°C. Afterward, 4μL of thiolated probe (400 pmol of oligonucleotide in immobilization buffer) was added and incubated at 4 °C for 12 h using 1 μL of 5μM of a reducing agent, tris (2-carboxyethyl) phosphine (TCEP). After washing with PBS buffer (0.01 M), 5 μL of 2-ME (0.2 mM) was added to each modified electrode. Before electrochemical measurement, 3% bovine serum albumin (BSA) was added to electrodes and incubated for half an hour. Finally, the hybridization process was performed by adding 5μl of *E. bieneusi* DNA (4ng/ml) in 20μL of DNA hybridization buffer (10 mM Tris–HCL, 30 mM $MgCl_2$, 1 mM EDTA, as well as 50 mM NaCl) to each of the probe-modified electrodes. Following a 45 min incubation at 37 °C, Tris buffer was used to wash the electrodes. The electrodes were then subjected to electrochemical analysis using DPVs and CV with scan rate of 50 mV/s, while the potential range of CV was + 0.2 to + 0.8 V (Fig. 2).

Electrode modification

The SPGEs had a gold working electrode with a disk (2 mm in radius), a silver pseudo-reference electrode, and a carbon counter electrode, while it was 1 cm in width, 3.4 cm in length, as well as 0.05 cm in height [58]. After preparation of working electrode, 10 μL of the as-synthesized Ti3C2/AuNPs/PDA nanocomposite (25μg/μl)

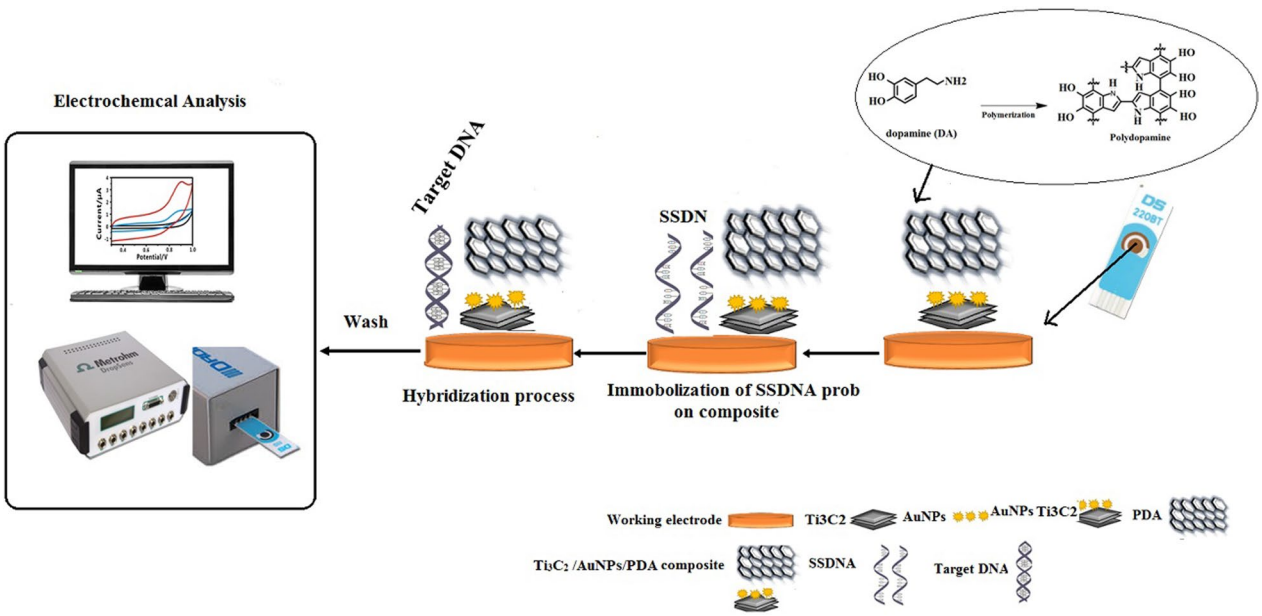

Fig. 2 Schematic presentation of electrochemical recognition strategy for detection of *E. bieneusi* DNA

was dropped on SPGEs and allowed to dry at 25°C. The disulfide bonds in 4μL of thiolated probe (400 pmol of oligonucleotide in immobilization buffer) were reduced after being incubated at 4 °C for 12 h using 1 μL of 5 μM of a reducing agent TCEP [59]. An immobilization buffer (10 mM Tris–HCL, 1 mM TCEP, 1 mM EDTA, as well as 50 mM NaCl, pH: 7.4) was a solution used to facilitate the attachment of biomolecules (e.g., nucleic acids, proteins) to a surface. This process is essential for the function of genosensors, which are designed to detect specific sequences of nucleic acids. Then, by employing the covalent bond of Au-sulfur, the thiol capture probe, which had been treated with TCEP, was immobilized on the surface of the Ti3C2/AuNPs/PDA modified electrode. After washing with PBS buffer (0.01 M), 5μl of 0.2 mM 2-ME was added on each modified electrode. Accordingly, the unreacted probe sites backfill with 2-ME. Finally, before performing electrochemical measurements, the 3% BSA was employed and incubated for 30 min. Finally, the surface of electrode was washed three times using ultrapure water [51, 60].

Hybridization process

To improve the sensitivity of DNA biosensors, it was crucial to immobilize the DNA probe, while preserving its natural affinity for the target DNA. Various techniques including adsorption, covalent bonding, microencapsulation, entrapment, and avidin–biotin interactions have been described for attaching DNA probes to electrode surfaces [20]. In this study the covalent immobilization process was included the creation of disulfide bonds between the enzyme's thiol groups and the disulfide oxide structures on the supports. The electron displacement surrounds the two sulfur atoms in disulfide oxides contributes to their high sulfur reactivity [61, 62]. Initially, the hybridization process was performed by mixing *E. bieneusi* DNA with DNA hybridization buffer. For the quantification of *E. bieneusi* DNA, 4 ng of *E. bieneusi* DNA (16 ng/mL) was prepared in 20μl of DNA hybridization buffer (10 mM Tris–HCL, 30 mM $MgCl_2$, 1 mM EDTA, as well as 50 mM NaCl, pH: 8.0) [59]. Afterwards, 5μl of prepared DNA hybridization buffer was added to each of the probe-modified electrode. Following a 45-min incubation at 37 °C, the Tris buffer was used to wash the electrodes, and they were subjected to electrochemical analysis (DPV) [63]. For the detection of *E. bieneusi* DNA, various concentrations of *E. bieneusi* DNA range from 0.1–10 ^{4} pg/mL, (0.1 pg, 0.5 pg, 10 pg, 50 pg, 100 pg, 500 pg, 1000 pg, 10000 pg/ml), were dropped onto the modified electrode and incubated at 37 °C for 45 min. Afterwards, the electrode was washed with PBS buffer and deionized water. The electrochemical signal was recorded via DPV, at the potential range of + 0.2 to + 0.8 V, the frequency of 15 Hz, and the amplitude of 0.05V using 5.0 mM [Fe(CN)6]−3/−4 containing 0.1 M KCl.

Electrochemical measurements

Using a $[Fe(CN)_6]^{3/4}$ solution, which contained 0.1M KCl as the redox-coupled probe, CV was used for the fundamental investigation of the electrode modification. Moreover, DPV was employed to assess how well the biosensor works. Experiments with CV and DPV were conducted using a scan rate of 50 mV/s as well as a potential range of + 0.2 to + 0.8 V, pulse amplitude of 0.05V, and pulse duration of 20ms [63]. Additionally, three different mismatch probe sequences were used to test the selectivity of the developed biosensor (Table 1). After 15 weeks of preservation at 4 °C, the modified electrodes'stability was compared to that of newly manufactured ones. Furthermore, the sensing procedure's reproducibility was evaluated by measuring two different concentrations in separate tests.

The LoD determination and specificity analysis

In order to calculate LoD of *E. bieneusi,* a series of standard solutions with different concentrations of the target analyte was prepared. The standard solution was measured using the established analytical method. In this regard, eight serial dilutions were prepared for a *E. bieneusi*-positive DNA sample by $\log^{-10}$, and the peak current or response for each concentration was then recorded. This data was plotted to generate a calibration curve. The calibration curve was analyzed to determine the linear range and the point at which the response begins to plateau or deviate. We calculated the standard deviation (SD) of the blank (i.e., the response when no analyte is present) over three repeats. The linear regression analysis was used to derive the equation of the line. The LoD was then calculated based on the previously published formula [64, 65]: 3SD/m, where the mean and SD are derived from replicate measurements of blank samples, and m is the slope of the calibration curve.

Results and discussion

Characterization of Ti3C2/AuNPs/PDA nanocomposite

The morphological criteria of the modified electrodes by Ti3C2/AuNPs/PDA nanocomposite were characterized using SEM. The SEM analysis revealed the layered accordion-like architecture of Ti3C2 and transparent nanoflakes stacked on each layer of Ti3C2 nanosheets (Fig. 3), as reported elsewhere [66]. After the immobilization of AuNPs on Ti3C2, the spherical morphology of AuNPs on Ti3C2 nanosheets was seen on the surface of SPGEs, including arrays of nanoparticles with 40–100 nm at high magnification. The SEM images of the Ti3C2/AuNPs/PDA nanocomposite structure showed that in addition to the presence of Ti3C2 nanosheets, AuNPs and PDA

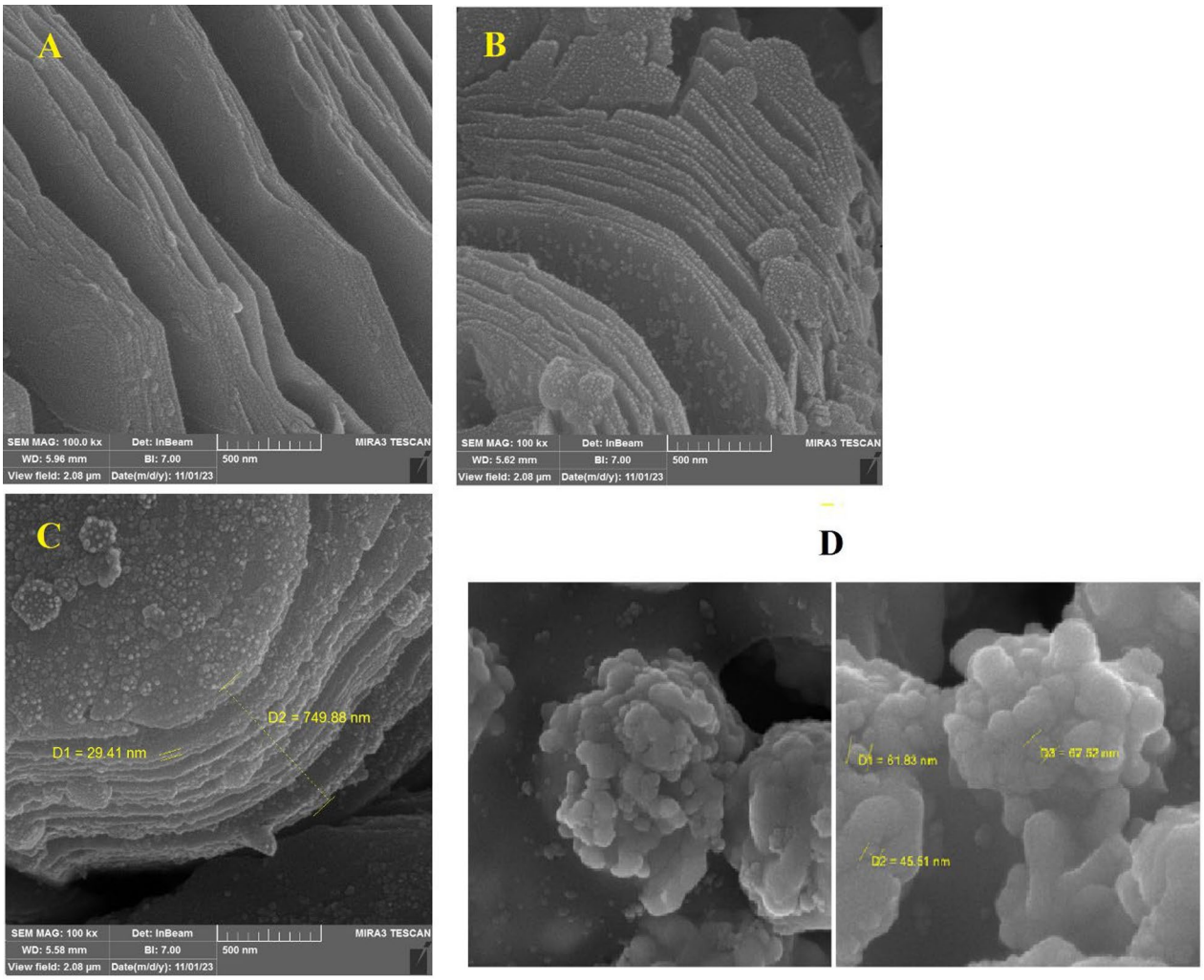

Fig. 3 The SEM images of **A** Ti3C2 nanosheets with accordion-like shape, possessing the unique layered structure with exfoliated sheets smooth surface, **B** AuNPs nanoparticles, displaying a generally spherical shape, **C** AuNPs between and at the edges of the Ti3C2 layers, increasing the interlayer spacing due to decoration of AuNPs between the Ti3C2 nanosheets, and **D** Ti3C2/AuNPs/PDA added on SPGE, showing that Ti3C2-MXene nanosheets were evenly covered with spherical PDA and AuNPs, while the ordered layer structure of Ti3C2-MXene was still retained. Upon combining with AuNPs/PDA, the surface of Ti_3C_2-MXene was became notably rough, with some AuNPs and PDA particles covering the surface of Ti_3C_2-MXene

shapes were observed among the sheets [67]. The TEM image confirmed deposition of composite-coated on substrates, in which Ti3C2 with HF and AuNPs were synthesized and well homogenized with the polymer, and were suitable for modifying the electrode surface (Fig. 4).

Available data has suggested Ti3C2-based composites as great materials for electrode modification and effective immobilization of biomolecule in electrochemical biosensor [68, 69]. In recent years, Ti3C2/AuNP composites have received rapid development by incorporating the advantageous of Ti3C2 and AuNPs to employ in electrical biosensor [70–77].

In the current study, the EDS mapping analysis revealed that the common elements in synthesized nanocomposite were: C, Ti, O, and F, and the constituent elements of Ti3C2 included C, Ti, O, F, AL, S. In addition, the EDS analysis showed the presence of the gold elements (Au, Si, S, C), which confirmed combination of the gold nanoparticles with AuNPs. As well, beside the constituent elements of AuNPs with Ti3C2, the essential elements of DA such as Cl, Na, Mg were observed. Due to the presence of DA elements along with AuNPs/Ti3C2 components, the synthesis of

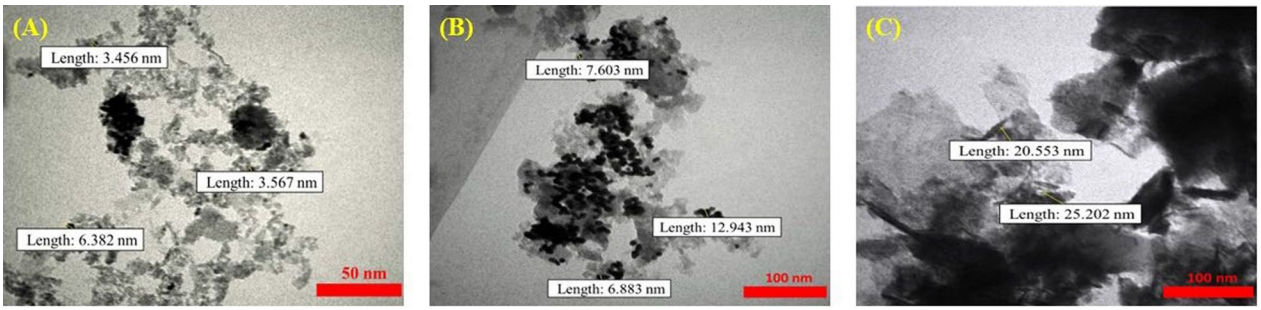

Fig. 4 The TEM image of nanocomposites of **A** Ti3C2/AuNPs/PDA; The labeled darker spots loading on the Ti3C2/AuNPs layers were PDA. **B** Ti3C2/AuNPs; The plentiful dark dots on Ti3C2 surface were Au nanoparticles, and **C**) Ti3C2; the layered structure was clearly found with unique 2D structure, while the sample consisted of few-layer flakes

Ti3C2/AuNPs/PDA nanocomposites was confirmed (Fig. 5).

The FT-IR spectroscopy showed that the functional groups of Ti3C2/AuNPs/PDA nanocomposite at the peaks around 3723 and 3300 cm^{-1} were related to hydroxyl groups that can be observed in all samples, while the functional groups C = O were observed at peak 1709 cm^{-1} and 1525 (Fig. 5E). The peaks of 1322 and 1372 cm^{-1} were related to the O–H bond, while the 572 cm^{-1} and 883 cm^{-1} were related to the vibrations of the oxygen group. All the peaks of Ti3C2/AuNPs were observed in the Ti3C2/AuNPs/PDA nanocomposite spectra. The IR absorption spectra of Ti3C2/AuNPs showed three broad peaks corresponding to vibrational bands at 3400–3800, 1661, and 1221 cm^{-1}. These were assigned to the adsorbed OH/H_2O on the NPs surface, because these bands were not observed alone in the Ti3C2 nanosheets. In contrast, vibrational bands at 450–780 cm^{-1} were observed alone in Ti3C2 nanosheets. According to the IR absorption spectra, the peaks in the range of 500 to 1000 cm^{-1} were seen in Ti3C2 (blue peak) [78], but these peaks were reduced when combined with nanoparticle (green peak). Also, there was a decrease in the peaks related to nanocomposite (red peak) compared to other cases. These results showed a successful combination and deposition of components on electrode, while significant differences for each stage of coating was observed. The vibrations around 2900 cm^{-1} in the Ti3C2 were also seen in the nanocomposite, while the vibrations around 500 cm^{-1} in the nanocomposite (red peak) were completely diminished.

Decomposition of polymer to Ti3C2/AuNPs was led to decrease in the amount of vibration, which was observed in the red color curve. Most of the bonding groups in the Ti3C2/AuNPs/PDA composite were related to oxygen and hydroxyl.

Characterization of modified electrodes

Electrochemical method

Until now, a couple of electrochemical biosensors have been developed for parasitic diseases (Table 2). In this study we evaluated Ti3C2/AuNPs/PDA nanocomposite for the first time to modify electrode surface and increase sensitivity of the system.

In order to characterize the surface of modified electrode, the CV and DPV electrochemical methods were applied. The CV curves obtained from the steps of modifications of SPGEs in a mixture solution of 5 mM $[Fe(CN)_6]^{3/4}$containing 0.1 M KCl have been observed (Fig. 6). As shown, when the surface of electrode was modified by the assembly AuNPs/Ti3C2, the peak current was increased due to the high conductivity and electron swift of AuNPs and Ti3C2, which improved the electrochemical features, owing to its large and electroactive surface area properties and great electrical conductivity (green peak) compared to the bare electrode (pink curve). It has been proven that the accordion-like nanoflake structure and the abundant surface functional groups of Ti3C2 offer a spacious surface for the loading of enzymes and nucleic acids, facilitating improved target detection [67]. The Ti3C2 amplified the current on the surface of the electrode, due to functional groups such as oxygen and fluorine. The Ti3C2 was significantly contributed to the electrochemical performance through their unique properties, including high conductivity and extensive surface area. The thiol-Au binding enhanced this performance by promoting efficient electron transfer and improving stability. This combination maximizes the electrochemical capabilities of Ti3C2 [66, 67]. The attachment of thiolated probe with AuNPs was due to the presence of the thiol group, which enhanced conductivity. Therefore, when Ti3C2 was used alone without AuNPs, a decrease in the sensitivity and conductivity of the biosensor system was seen (dark blue). Moreover, it was seen that the increased current peak of composite (red

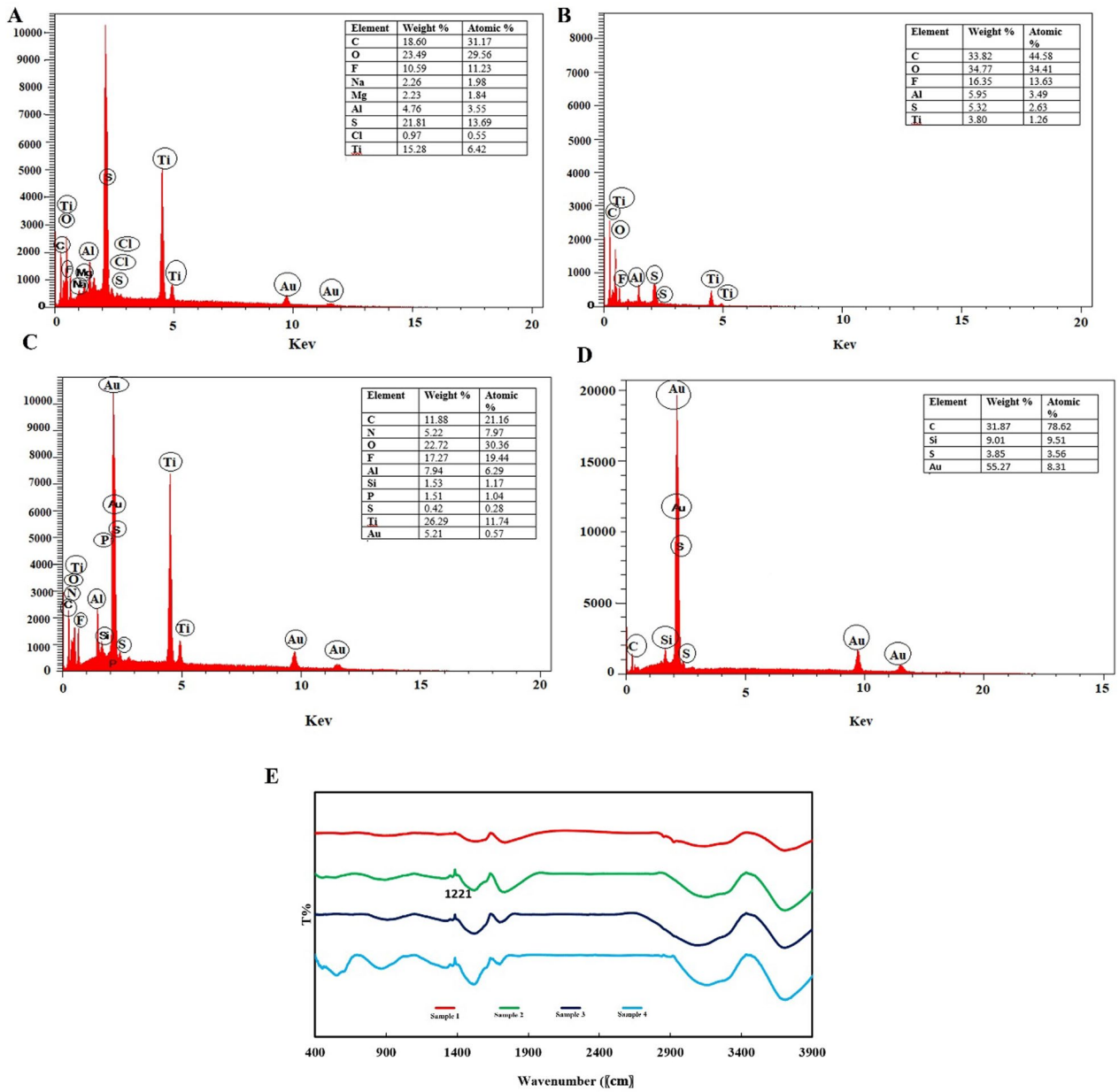

Fig. 5 Elemental mapping, EDS spectrum, and quantitative analysis of elemental composition of Ti3C2/AuNPs/PDA nanocomposite. **A** Ti3C2/AuNPs/PDA nanocomposite, **B** Ti3C2, **C** Ti3C2/AuNPs, **D** AuNPs, and **E** FT-IR spectrum of Ti3C2/AuNPs/PDA nanocomposite. **Sample 1**: Ti3C2/AuNPs/PDA nanocomposite, **Sample 2:** Ti3C2/AuNPs, **Sample 3:** AuNPs, and **Sample 4:** Ti3C2

peak) was attributed to the large surface area and electric conductivity of nanocomposite [37]. The increased current intensity indicated excellent electrical conductivity between nanocomposite and the negative charge of $[Fe(CN)_6]^{3/4}$. Upon the thiolated probe ssDNA was immobilized on modified electrode (AuNP/Ti3C2/PDA/Probe), the signal current was decreased in present of the $[Fe(CN)_6]^{3/4}$ (light blue peak). This result was due to the negative charge of thiolated-ssDNA and $[Fe(CN)_6]^{3/4}$, which caused electrostatic repulsion between probe and substrate [20]. In addition, the electron transfer was blocked due to the hybridization of DNA and the electrode [82]. The electrode surface, covered by thiolated-ssDNA, decreased electron transfer and prevented the transfer of redox molecules to electrodes surface. The decrease in the peak current values by the addition of *E. bieneusi* DNA might be attributed to the formation of DNA—ssDNA complex that increased the resistance

Table 2 Summary of the various biosensors is employed for detection of parasites

Detection principle	Target analyte	Linear and LoD	Propertices	Refs.
• A label-free electrochemical genosensor using a probe and a conductive Mxene-Ti3C2/AuNPs/PDA as electrode substrate	*E. bieneusi*	0.1–10 ^{4} pg mL-1	• A thiolated probe oligonucleotide	Current study
• Without redox marker		(LOD) of 0.06 fg/mL	• High sensitivity and selectivity, and low-cost	
• Screen printed gold electrode (SPGE) to facilitate attachment of thiolated probe oligonucleotide			• Miniaturization capability	
• Hybridization of the complementary single stranded DNA sequence			• Using two dimensional (2D) materials and nanoparticles with PDA to improve the conductivity of surface	
• Cyclic voltammetry (CV) and differential pulse voltammograms (DPVs) electrochemical methods			• The integration of Ti3C2 and Gold nanoparticles to facilitate the effective immobilization of DNA, and improve the overall electron transfer kinetics	
			• Specific detection	
			• Label-free and PCR-free	
• Electrochemical genosensor based on hybridization of the complementary single stranded DNA sequence	*Trichomonas vaginalis*	• 1.0×10^{-19} to 1×10^{-12} mol L – 1	• A thiolated probe oligonucleotide	[64]
		• LOD: 3.1×10^{-20} mol L – 1	• High sensitivity and selectivity, and low-cost	
• Toluidine blue as a redox marker			• Label-free and PCR-free	
			• Gold nanoparticles as a platform as a ultrasensitive electrochemical genosensor	
			• High stability and good biocompatibility	
• Electrochemical impedance spectroscopy (EIS) screen printed carbon electrode (SPCE)	*L. donovani*	• 2 pg/ml to 2 µg/ml	• Graphene have been successfully used in impedimetric biosensors	[79]
• Nickel oxide (NiO) film deposited onto indium tin oxide (ITO) coated glass plate		• LOD:0.02 ng/µl	• A polythionine layer was electrodeposited on the surface increases resistivity, rough surface, and the conductivity	
• Methylene blue (MB), a well-known hybridization indicator of DNA			• IrO_2 NPs show suitable redox properties	
			• Non-covalent bond formation between surface with amino groups on the biomolecule	
• Labeled electrochemical sensor,	*C. parvum*	• 150 to 800 oocysts, LOD: 100 oocysts	• The high sensitivity and specificity of the aptamers	[80]
• Gold nanoparticle-modified screen-printed carbon electrode				
• Self-assembled monolayer of a thiolated-DNA capture probe				
• Square wave voltammetry was employed to quantitate *C. parvum*				
• Thiolated-DNA capture probe and an oocyst-specific DNA aptamer onto a gold nanoparticle				

Table 2 (continued)

Detection principle	Target analyte	Linear and LoD	Propertices	Refs.
• Electrochemical DNA biosensors	*L. major*	• 1.0×10^{-10} to 1.0×10^{-19} mol L-1	• Simple, rapid, accurate and low cost methods	[81]
• Gold nanoleaves		• LOD: 1.8×10^{-20} mol L-1	• Differentiate between *L. major* and *L. tropica*	
• Methylene blue was the marker			• High selectivity	
• Hybridization of the complementary single stranded DNA sequence			• Label-free, PCR-free	

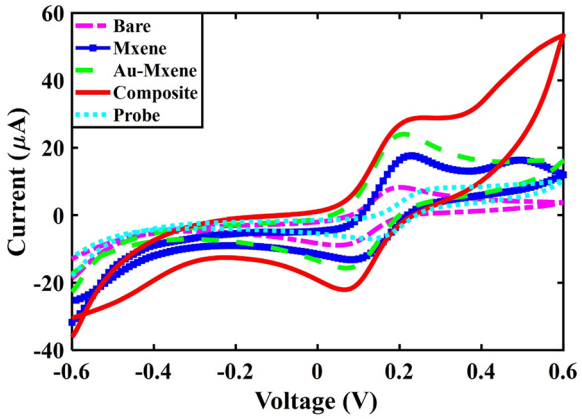

Fig. 6 Cyclic voltammogram of modified electrode measured in 5.0 mM [Fe $(CN)_6$] $^{3-/4-}$ containing 0.1 M KCl at a scan rate of 100 mV/s for bare SPCE (pink), AuNP/Ti3C2 modified SPGE (green), Ti3C2/AuNPs/PDA @SPGE modified SPCE (red), after immobilization of thiolated probe on Ti3C2/AuNPs/PDA @SPGE modified SPCE (blue), and Ti3C2, which was only modified SPGE (dark blue). Each data point represents the average of three replicates

to [$Fe(CN)_6$] $^{3-/4}$ molecules to cross through this complex, and decreased the number of its molecules, which reacted with the electrode surface. Figure 7 illustrates the CV curve obtained from the bare electrode and different modified SPGEs in presence of 1 mM [$Fe(CN)_6$]$^{3/4}$ (Fig. 7). The CV curve showed that upon adding target DNA (100 ng/ml), the peak current was declined due to proper hybridization between the probe and target DNA (Fig. 6).

In CV analysis, along with the increase in DNA concentration from 0.1 pg/ml to 10 ng/ml (0.1 pg, 0.5 pg, 10 pg, 50 pg, 100 pg, 500 pg, 1000 pg, 10000 pg/mL), the DPV responses of [$Fe(CN)_6$] $^{3-/4}$ oxidation indicated decrease in the current intensity, which was related to the blocking of the electrode surface by the DNA concentrations on the modified electrode. This finding suggested that the intensity current was directly related to the amount of the target DNA concentration in the sample. Accordingly, the highest concentration of target DNA was exhibited lowest current (Fig. 7A).

A logarithmic correlation between the changes in the DPV peak currents (ΔIs) and *E. bieneusi* DNA concentration was seen. The linear relationship between the changes in the DPV peak currents ΔI (μA) and log (*E. bieneusi* DNA concentration) (pg/mL) in the DNA concentrations ranged from 0.1 to 10^{4} pg/mL, 0.1 pg, 0.5 pg, 10 pg, 50 pg, 100 pg, 500 pg, 1000 pg, 10000 pg/mL with a linear regression equation of y= 5.2689x +7.688, ΔI (μA) =5.2689 log (concentration) (pg/mL) +7.688 and correlation coefficient of 0.991 (Fig. 7B) [83]. As shown in Fig. 7C, there was a significant decrease in the corresponding peak current with increasing *E. bieneusi* DNA concentrations.

The LOD was calculated by this formulation; 3 SD/m, SD is the standard deviation of blank signal (peak current in the absence of DNA), and m is the slope of the regression equation (y =5.2689x +7.688) with a limit of detection of 0.06 pg/mL for DNA detection.

Optimization of AuNPs/Ti3C2/PDA composite concentration on the SPGE

To optimize nanocomposite on electrode, the concentrates 25, 50, 75, 100 (μg/mL) were prepared and electrochemical characteristic (CV mode) was obtained using 10 μL from each concentration with Ferricyanide [Fe $(CN)_6$] $^{3-/4}$ 0.1 M, as an oxidant agent on the surface of electrodes. The current was directly proportional to the concentration of the composite, resulting in an increase in current along with an increase in the electrode surface due to elevated charge density on the electrode surface. The analysis of the findings indicated that the ideal concentration of the composite was 25 μg/mL. Therefore, the optimized concentration was assigned and 10 μL (25 μg/mL) of nanocomposite was dropped on each electrode and incubated at 25 °C (Fig. 8A). In order to optimize the probes concentration on modified SPGE, different amounts of probe (2, 4, 6, μM/mL per electrode) were employed. The results demonstrated that increasing the amount of probe concentration was led to an enhancement in the current signal intensity; however, due to the low intensity variation between 4 and 6 μM/mL, 4 μM/mL was chosen as the optimal amount for this assay. The current signal was increased by enhancing the concentration of the probe and reach to a plateau at 6 mL concentration. Accordingly, a saturation of the modified electrode surface with probe occurred at 4 μM/mL of probe and this concentration could be regarded as the optimum probe concentration. Subsequently, 5 μL from 4 μM/mL of probe was coated onto AuNPs/Ti3C2/PDA modified electrodes, which were incubated for 12 h at 4 °C (Fig. 8B).

Selectivity, reproducibility, and stability of the AuNPs/Ti3C2/PDA composite

Reproducibility and stability are critical characteristics for a biosensor in real applications.

Selectivity

In this study, to evaluate the selectivity of the current biosensor, we repeated the test with different parasite as non-specific DNA, including *Giardia lamblia* (1ng/mL) as a protozoan and *Trichostrongylus* sp. (1ng/mL) as a helminthic parasite. The relative standard deviation (RSD) values of *G. lamblia*, *Trichostrongylus* sp., and *E.*

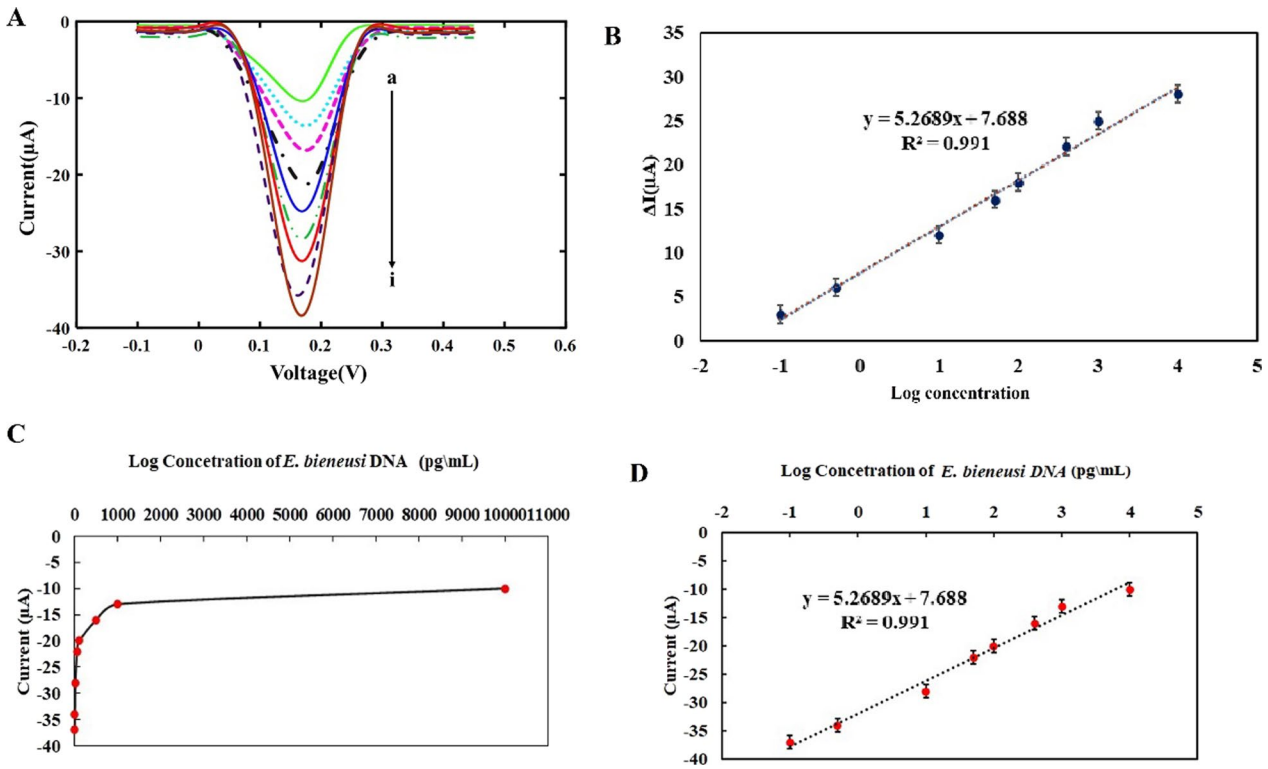

Fig. 7 **A** Typical differential pulse voltammograms response of [0.1M KCl and 1 mM Fe $(CN)_6]^{3-/4-}$ oxidation after adding *E. bieneusi* DNA at probe/Ti3C2/AuNPs/PDA SPGE toward multiple detection of serial concentrations of *E. bieneusi* DNA of 0.1 pg, 0.5 pg, 10 pg, 50 pg, 100 pg, 500 pg, 1000 pg, 10000 pg, (a–i): $0.1–10^4$ pg/mL **B** Calibration curve of a logarithmic correlation between the changes in the DPV peak currents (ΔIs) and *E. bieneusi* DNA concentration. **C** Variation of the biosensor responses against the *E. bieneusi* concentrations in the range of $0.1–10^4$ pg/mL. The image shows the linear relationship between the peak currents and *E. bieneusi* DNA concentrations. The illustrated error bars represent the standard deviation of three repetitive measurements. **D** Calibration curve of a logarithmic correlation between the peak currents and *E. bieneusi* DNA concentration

bieneusi were 4.7%, 4.54%, and 3.09%, respectively. As demonstrated (Fig. 9A), replacing the target DNA with genetic materials of other parasites than *E. bieneusi*, with interfering components, provided only weak signals, indicating high specificity of the current biosensor for detecting *E. bieneusi* [84]. In addition, the mismatch analysis showed that the biosensor could discriminate our target from mismatches in the hybridization sequence, indicating the excellent selectivity and ability to distinguish the hybridization detection from mismatched target sequences (Fig. 9B).

Stability

In order to investigate of inter-electrode stability of biosensor, 500 fg (0.5pg) of DNA was examined on several electrodes at 4 °C for 5 weeks. The electrochemical responses were measured every week. After a period of 5 weeks, the current of CV showed an identical response for electrodes, when was compared to freshly prepared electrodes. The acceptable RSD value (2.7%) confirmed the reasonable stability of the modified surfaces of the assay (Fig. 9C).

Reproducibility

In order to evaluate the reproducibility (intra-assay) of the developed biosensor, electrochemical analysis was conducted. Accordingly, repeated measurements were conducted on both the same modified electrode and four different electrodes, under identical conditions. To determine the repeatability, three concentrations of composite were fabricated (50, 500, 1000 pg/mL) and repeated for five times, which resulted RSD values of 1.2%, 1.3% and 1.8%, respectively. Subsequently, the biosensor exhibited an excellent reproducibility for target determination (Fig. 9D).

Conclusion

In conclusion, the electrochemical determination of *E. bieneusi* DNA, utilizing a screen-printed gold electrode modified with Ti3C2, AuNPs, and PDA demonstrated a significant advancement in detection of *E. bieneusi*.

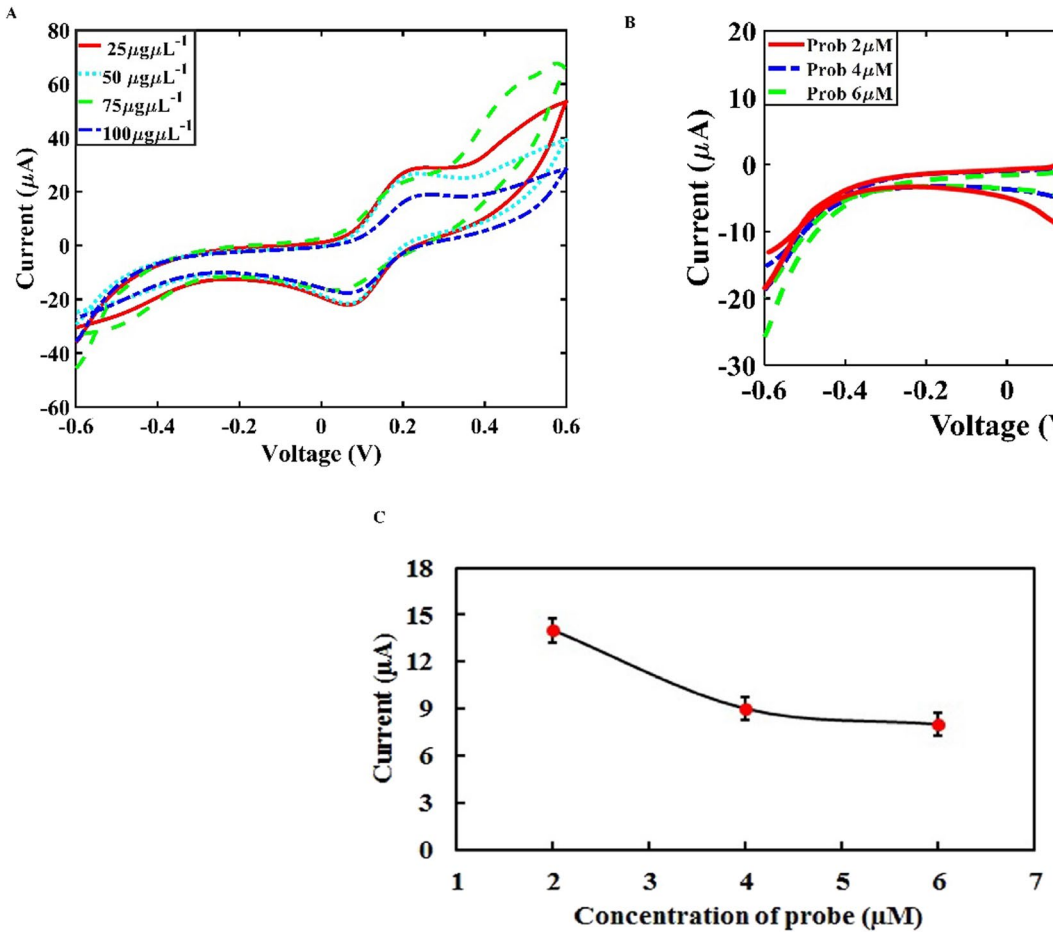

Fig. 8 **A** Optimization of Au/Ti3C2/PDA composite concentration on the Au@SPGE with 25,50, 75 and 100 µg/mL. **B** Optimization of probes on PDA/Au/Ti3C2 composite on Au@SPGE, with 2,4,6, µM concentrates. **C** Optimization of concentrations of probe according to current. Error bars were achieved based on three independent measurements

This innovative sensor configuration enhanced the electrochemical properties and selectivity for the specific detection of *E. bieneusi* DNA, contributing to improved sensitivity and accuracy. The integration of Ti3C2 and AuNPs seems not only facilitated the effective immobilization of DNA, but also improved the overall electron transfer kinetics, resulting in a formidable platform for genetic diagnostics. In addition, the developed biosensor demonstrated excellent sensitivity and selectivity, achieving a LoD of 0.06 pg/mL, with high selectivity.

Future applications of this technology could be extend beyond *E. bieneusi* detection, potentially serving as a blueprint for developing rapid and efficient assays for other pathogens. This biosensor could be developed as a disposable one-use, cheap, and rapid electrochemical biosensor. The promising results suggest that this electrochemical approach could play a vital role in public health monitoring and environmental surveillance.

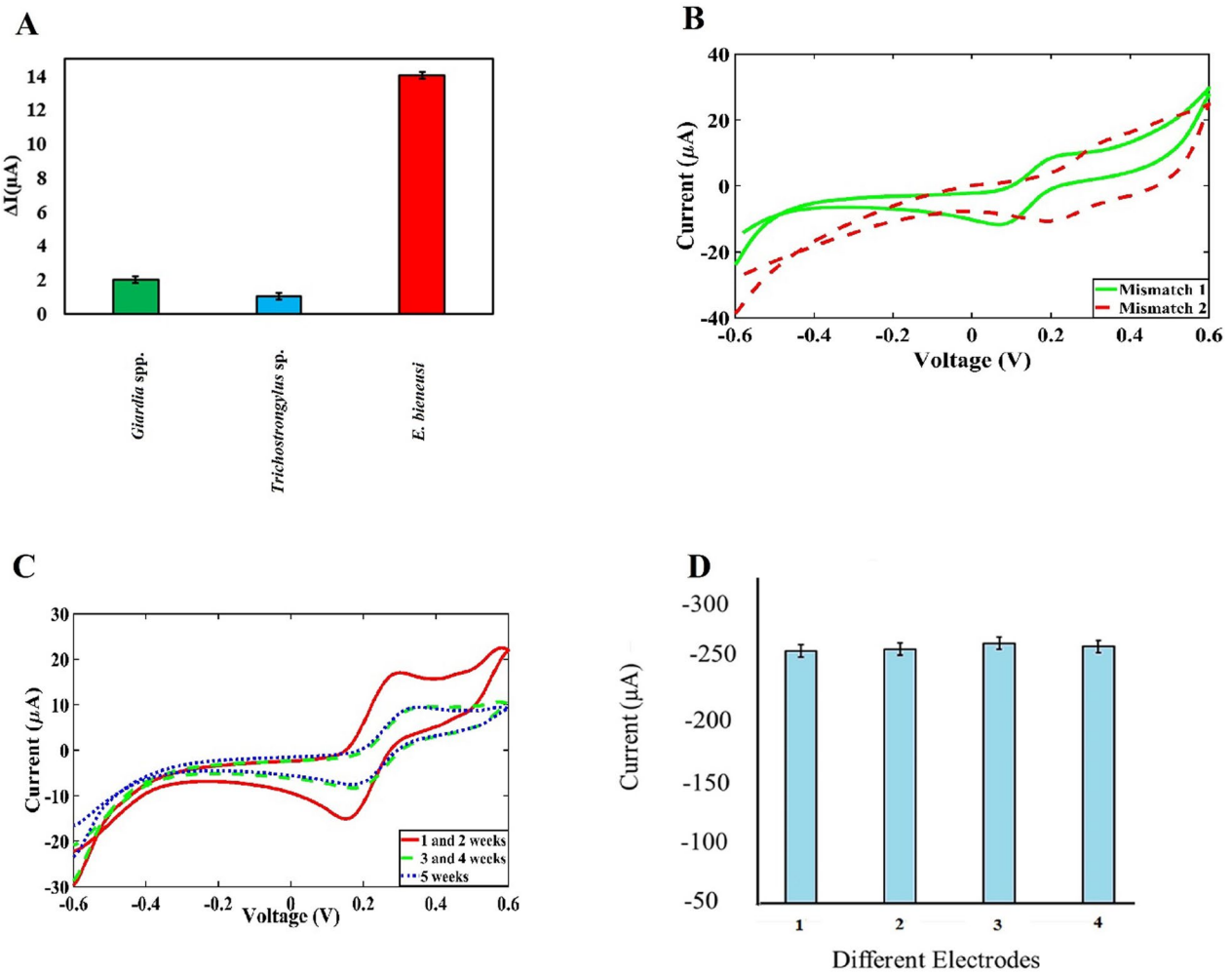

Fig. 9 **A** Selectivity test of the developed biosensor in presence of various types of interference proteins (*Trichostrongylus* sp., and *G. lamblia*). Error bars were achieved based on three independent measurements. **B** The mismatch analysis showed that the biosensor discriminated the target from mismatches in the hybridization sequence. **C** The stability of the biosensor was tested in five weeks at 4 ºC, and **D** Reproducibility (inter-assay) analysis of the biosensor using four different electrodes incubated with 200 pg/mL. Error bars were achieved based on three independent measurements

Acknowledgements
The authors thank all members of the Foodborne and Waterborne Diseases Research Center for their collaborations.

Author contributions
HM designed the study. SN and HMR contributed molecular tests. SN and SMK contributed in synthesis and tests. KO and SN contributed confirmation analysis. AS provided facilities. HM and SN contributed in manuscript writing. All authors read and confirmed the final version of the manuscript.

Funding
This study was financially supported by the Research Institute for Gastroenterology and Liver Diseases, Shahid Beheshti University of Medical Sciences with grant number: RIGLD- 1126.

Availability of data and materials
All data generated or analyzed during this study are included in this published article.

Declarations

Ethics approval and consent to participate
Because of employing *E. bieneusi* sample from human cases, this project was approved by the Ethical Review Committee of the Research Institute for Gastroenterology and Liver Diseases, Shahid Beheshti University of Medical Sciences, Tehran, (IR.SBMU.RIGLD.REC.1399.044). The samples were purified DNA, which had been stored in the sample bank of the Parasitology, Mycology, and Water Research Lab, Foodborne and Waterborne Diseases Research Center, Research Institute for Gastroenterology and Liver Diseases, Shahid Beheshti University of Medical Sciences. However, informed consent had been obtained from participants or legal guardians of any participant under the age of 16 and sampling followed the Declaration of Helsinki.

Consent for publication
Not applicable.

Transparency statement
Corresponding authors affirm that this manuscript is an honest, accurate, and transparent account of the study being reported; that no important aspects

of the study have been omitted; and that any discrepancies from the study as planned (and, if relevant, registered) have been explained.

Competing interests
The authors declare no competing interests.

Author details
[1]Foodborne and Waterborne Diseases Research Center, Research Institute for Gastroenterology and Liver Diseases, Shahid Beheshti University of Medical Sciences, Tehran, Iran. [2]Gastroenterology and Liver Diseases Research Center, Research Institute for Gastroenterology and Liver Diseases, Shahid Beheshti University of Medical Sciences, Tehran, Iran. [3]Department of Chemistry, Faculty of Basic Sciences, Ayatollah Boroujerdi University, Boroujerd, Iran. [4]Biosensor Research Center, Endocrinology and Metabolism Molecular–Cellular Sciences Institute, Tehran University of Medical Sciences, P.O. Box 14395/1179, Tehran, IR, Iran. [5]Endocrinology and Metabolism Research Center, Endocrinology and Metabolism Research Institute, Tehran University of Medical Sciences, Tehran, Iran.

Received: 1 February 2025 Accepted: 4 June 2025
Published online: 02 July 2025

References

1. Didier ES, et al. Microsporidiosis in mammals. Microbes Infect. 2000;2(6):709–20.
2. Han B, Pan G, Weiss LM. Microsporidiosis in humans. Clin Microbiol Rev. 2021;34(4): e0001020.
3. Franzen C, Müller A. Microsporidiosis: human diseases and diagnosis. Microbes Infect. 2001;3(5):389–400.
4. Weiss LM. The microsporidia and microsporidiosis. 1999: ASM Press.
5. Didier ES, Weiss LM. Microsporidiosis: not just in AIDS patients. Curr Opin Infect Dis. 2011;24(5):490–5.
6. Nourrisson C, et al. *Enterocytozoon bieneusi*, a human pathogen. Emerg Microbes Infect. 2024;13(1):2406276.
7. Didier ES, et al. Epidemiology of microsporidiosis: sources and modes of transmission. Vet Parasitol. 2004;126(1–2):145–66.
8. Han B, Weiss Louis M. Microsporidia: obligate intracellular pathogens within the fungal kingdom. Microbiol Spectr. 2017. https://doi.org/10.1128/microbiolspec.funk-0018-2016.
9. Karimi K, et al. Molecular epidemiology of *Enterocytozoon bieneusi* and *Encephalitozoon* sp., among immunocompromised and immunocompetent subjects in Iran. Microb Pathog. 2020;141:103988.
10. Hasani Z, et al. The first study on opportunistic intestinal microsporidiosis in IBD patients receiving immunosuppressive medications in Iran. Epidemiol Infect. 2017;145(10):2095–9.
11. Javanmard E, et al. Molecular and phylogenetic evidences of dispersion of human-infecting microsporidia to vegetable farms via irrigation with treated wastewater: One-year follow up. Int J Hyg Environ Health. 2018;221(4):642–51.
12. Li T, et al. CRISPR/Cas9 therapeutics: progress and prospects. Signal Transduc Target Therap. 2023;8(1):36.
13. Wang T, et al. Next-generation CRISPR-based diagnostic tools for human diseases. TrAC Trends in Analyt Chem. 2023;168: 117328.
14. Nemati S, et al. Toward waterborne protozoa detection using sensing technologies. Front Microbiol. 2023;14:1118164.
15. Vigneshvar S, et al. Recent advances in biosensor technology for potential applications—an overview. Front Bioengin Biotechnol. 2016. https://doi.org/10.3389/fbioe.2016.00011.
16. Chadha U, et al. Recent progress and growth in biosensors technology: a critical review. J Indust Engin Chem. 2022;109:21–51.
17. Cho I-H, Kim DH, Park S. Electrochemical biosensors: perspective on functional nanomaterials for on-site analysis. Biomaterials Res. 2020;24(1):6.
18. Vidic J, et al. Advanced biosensors for detection of pathogens related to livestock and poultry. Vet Res. 2017;48(1):11.
19. Cesewski E, Johnson BN. Electrochemical biosensors for pathogen detection. Biosens Bioelectron. 2020;159: 112214.
20. Shoaie N, Forouzandeh M, Omidfar K. Voltammetric determination of the Escherichia coli DNA using a screen-printed carbon electrode modified with polyaniline and gold nanoparticles. Mikrochim Acta. 2018;185(4):217.
21. Jin S, Porterfield DM, surface modification approaches for electrochemical biosensors, in Biosensors, S. Pier Andrea, Editor. 2011, IntechOpen: Rijeka. 11.
22. Thulasiprevinnah S, et al. Recent advances in electrochemical biosensors for the determination of biomolecules on modified and unmodified electrodes. J Iran Chem Soc. 2024;21(7):1739–68.
23. Long JJ, et al. Polymers in biosensors. In: Amid A, et al., editors. multifaceted protocol in biotechnology. Singapore: Springer Singapore; 2018. p. 151–65.
24. Viswanathan S, Radecka H, Radecki J. Electrochemical biosensors for food analysis. Monatshefte Chem Chem Month. 2009;140:891–9.
25. Fu J, et al. Electrochemical aptasensor based on one step co-electrodeposition of aptamer and GO-CuNPs nanocomposite for organophosphorus pesticide detection. Sensor Actuat B: Chem. 2019;287:503–9.
26. Rocha JF, Hasimoto LH, Santhiago M. Recent progress and future perspectives of polydopamine nanofilms toward functional electrochemical sensors. Analyt Bioanalyt Chem. 2023;415(18):3799–816.
27. Varol HS, et al. Electropolymerization of polydopamine at electrode-supported insulating mesoporous films. Chem Material. 2023;35(21):9192–207.
28. Lee HA, et al. Material-independent surface chemistry beyond polydopamine coating. Account Chem Res. 2019;52(3):704–13.
29. Ryu JH, Messersmith PB, Lee H. Polydopamine surface chemistry: a decade of discovery. ACS Appl Material Interfac. 2018;10(9):7523–40.
30. Delparastan P, et al. Direct evidence for the polymeric nature of polydopamine. Angewandte Chem Int Edition. 2019;58(4):1077–82.
31. Kund J, et al. Physicochemical and electrochemical characterization of electropolymerized polydopamine films: influence of the deposition process. Nanomaterials. 2021;11(8):1964.
32. Yoo YK, et al. Gold nanoparticles assisted sensitivity improvement of interdigitated microelectrodes biosensor for amyloid-β detection in plasma sample. Sensor Actuat B: Chem. 2020;308: 127710.
33. Xia N, et al. Design of electrochemical biosensors with peptide probes as the receptors of targets and the inducers of gold nanoparticles assembly on electrode surface. Sensor Actuat B: Chem. 2017;239:834–40.
34. Carneiro P, et al. Alzheimer's disease: Development of a sensitive label-free electrochemical immunosensor for detection of amyloid beta peptide. Sensor Actuat B: Chem. 2017;239:157–65.
35. Meng Z, et al. Electrically-transduced chemical sensors based on two-dimensional nanomaterials. Chem Rev. 2019;119(1):478–598.
36. Lorencova L, et al. Highly stable Ti3C2Tx (MXene)/Pt nanoparticles-modified glassy carbon electrode for H2O2 and small molecules sensing applications. Sensor Actuat B: Chem. 2018;263:360–8.
37. Lorencova L, et al. Electrochemical performance of Ti(3)C(2)T(x) MXene in aqueous media: towards ultrasensitive H2O2 sensing. Electrochim Acta. 2017;235:471–9.
38. Yang G, et al. MXenes-based nanomaterials for biosensing and biomedicine. Coordinat Chem Rev. 2023;479: 215002.
39. Wang Q, et al. MXene-based electrochemical (bio) sensors for sustainable applications: roadmap for future advanced materials. Nano Material Sci, 2022.
40. Yang X, et al. An electrochemical biosensor based on AuNPs/Ti3C2 MXene three-dimensional nanocomposite for microRNA-155 detection by exonuclease III-aided cascade target recycling. J Electroanalyt Chem. 2020;878: 114669.
41. Deb VK, Jain U. Ti3C2 (MXene), an advanced carrier system: role in photothermal, photoacoustic, enhanced drugs delivery and biological activity in cancer therapy. Drug Deliver Translat Res. 2024;14(11):3009–31.
42. Luo W, et al. Biocompatibility nanoprobe of MXene N-Ti3C2 quantum dot/Fe3+ for detection and fluorescence imaging of glutathione in living cells. Colloid Surfac B: Biointerfac. 2021;201: 111631.
43. Wen Y, et al. Exposure to two-dimensional ultrathin Ti3C2 (MXene) nanosheets during early pregnancy impairs neurodevelopment of offspring in mice. J Nanobiotechnol. 2022;20(1):108.
44. Lee H, et al. Mussel-inspired surface chemistry for multifunctional coatings. Science. 2007;318(5849):426–30.
45. Lynge ME, Schattling P, Städler B. Recent developments in poly(dopamine)-based coatings for biomedical applications. Nanomedicine (Lond). 2015;10(17):2725–42.

46. Liu Y, Ai K, Lu L. Polydopamine and its derivative materials: synthesis and promising applications in energy, environmental, and biomedical fields. Chem Rev. 2014;114(9):5057–115.
47. Black KC, et al. Polydopamine-enabled surface functionalization of gold nanorods for cancer cell-targeted imaging and photothermal therapy. Nanomedicine (Lond). 2013;8(1):17–28.
48. Zeng Y, et al. Lipid-AuNPs@PDA nanohybrid for MRI/CT imaging and photothermal therapy of hepatocellular carcinoma. ACS Appl Material Interfac. 2014;6(16):14266–77.
49. Sui J, et al. MXene derivatives: synthesis and applications in energy convention and storage. RSC Adv. 2021;11(26):16065–82.
50. Wu Q, et al. A 2D transition metal carbide MXene-based SPR biosensor for ultrasensitive carcinoembryonic antigen detection. Biosensor Bioelectron. 2019;144: 111697.
51. Norouzi Eshlaghi S, et al. A label-free electrochemical aptasensor based on screen printed carbon electrodes with gold nanoparticles-polypyrrole composite for detection of cardiac troponin I. IEEE Sensor J. 2023;23(4):3439–45.
52. Omidfar K, et al. A high-sensitivity electrochemical immunosensor based on mobile crystalline material-41–polyvinyl alcohol nanocomposite and colloidal gold nanoparticles. Analyt Biochem. 2012;421(2):649–56.
53. Li K, et al. Fabrication of tunable hierarchical MXene@AuNPs nanocomposites constructed by self-reduction reactions with enhanced catalytic performances. Sci China Mater. 2018;61(5):728–36.
54. Jandas PJ, et al. Ti3C2Tx MXene-Au nanoparticles doped polyimide thin film as a transducing bioreceptor for real-time acoustic detection of carcinoembryonic antigen. SensorActuat A Physic. 2021;331: 112998.
55. Ball V. Polydopamine films and particles with catalytic activity. Catal Today. 2018;301:196–203.
56. Xu M, et al. Polydopamine-coated gold nanoparticles used as modifier of the electron transport layer for PTB7:PC71BM polymer solar cells. J Material Sci: Material Electron, 2020. 31.
57. Sotoma S, Harada Y. Polydopamine coating as a scaffold for ring-opening chemistry to functionalize gold nanoparticles. Langmuir. 2019;35(25):8357–62.
58. Taleat Z, Khoshroo A, Mazloum-Ardakani M. Screen-printed electrodes for biosensing: a review (2008–2013). Microchim Acta. 2014;181(9):865–91.
59. Wu F, et al. Ratiometric detection of oligonucleotide stoichiometry on multifunctional gold nanoparticles by whispering gallery mode biosensing. Analyst. 2015. https://doi.org/10.1039/C5AN00179J.
60. Liu Y, et al. Immobilization strategies for enhancing sensitivity of electrochemical aptamer-based sensors. ACS Appl Mater Interfaces. 2021;13(8):9491–9.
61. Saberi R, Shahrokhian S, Marrazza G. Amplified electrochemical DNA sensor based on polyaniline film and gold nanoparticles. Electroanalysis. 2013;25:1373.
62. Monosik R, Streansky M, Surdik E. Biosensors-classification, characterization and new trends. Act Chim Slovaca. 2012;5:109–20.
63. Moradi M, et al. Electrochemical genosensing of Leishmania major using Gold hierarchical nanoleaflets. J Biol Today's World. 2016. https://doi.org/10.15412/J.JBTW.01050801.
64. Delshadi-Jahromi N, et al. Label-free ultrasensitive electrochemical genosensing of *Trichomonas vaginalis* using anisotropic-shaped gold nanoparticles as a platform, a repeated sequence of the parasite DNA as a probe, and toluidine blue as a redox marker. Sens Actuators, B Chem. 2018;273:234–41.
65. Heli H, et al. An electrochemical genosensor for *Leishmania major* detection based on dual effect of immobilization and electrocatalysis of cobalt-zinc ferrite quantum dots. Talanta. 2016;156–157:172–9.
66. Lorencova L, et al. MXene-based electrochemical devices applied for healthcare applications. Mikrochim Act. 2024;191(2):88.
67. Mohammadniaei M, et al. Gold nanoparticle/MXene for multiple and sensitive detection of oncomiRs based on synergetic signal amplification. Biosens Bioelectron. 2020;159: 112208.
68. Rakhi RB, et al. Novel amperometric glucose biosensor based on MXene nanocomposite. Sci Rep. 2016;6:36422.
69. Jiang X, et al. Pathogen-imprinted polymer film integrated probe/Ti3C2Tx MXenes electrochemical sensor for highly sensitive determination of *Listeria Monocytogenes*. J Electrochem Sci Technol. 2022;13(4):431–7.
70. Haddadi SA, et al. Amino-functionalized MXene nanosheets doped with Ce(III) as potent nanocontainers toward self-healing epoxy nanocomposite coating for corrosion protection of mild steel. ACS Appl Mater Interfac. 2021;13(35):42074–93.
71. He X, et al. A high-performance waterborne polymeric composite coating with long-term anti-corrosive property based on phosphorylation of chitosan-functionalized Ti3C2Tx MXene. Adv Composit Hybrid Mater. 2022;5(3):1699–711.
72. Wang L, et al. 3D Ti3C2Tx MXene/C hybrid foam/epoxy nanocomposites with superior electromagnetic interference shielding performances and robust mechanical properties. Compos A Appl Sci Manuf. 2019;123:293–300.
73. Li Y, et al. Ni0.6Zn0.4Fe2O4/Ti3C2Tx nanocomposite modified epoxy resin coating for improved microwave absorption and impermeability on cement mortar. Construct Build Mater. 2021;310:125213.
74. Jaffari Z, et al. Recent progress in Ti3C2Tx-based materials: from fundamentals to emerging applications. Material Sci Semiconduct Process. 2022;148: 106835.
75. Du X, et al. Dopamine-decorated Ti3C2Tx MXene/cellulose nanofiber aerogels supported form-stable phase change composites with superior solar–thermal conversion efficiency and extremely high thermal storage density. ACS Appl Material Interf. 2022;14(13):15225–34.
76. Fredi G, et al. Bioinspired polydopamine coating as an adhesion enhancer between paraffin microcapsules and an epoxy matrix. ACS Omega. 2020;5(31):19639–53.
77. Zmerli I, Michel J-P, Makky A. Bioinspired polydopamine nanoparticles: synthesis, nanomechanical properties, and efficient PEGylation strategy. J Material Chem B. 2020;8(20):4489–504.
78. Yu C, et al. Facile Preparation of Ti 3 C 2 T x MXene@Zn–Mn ferrite composites with enhanced microwave absorption performance. ACS Appl Electron Mater. 2022. https://doi.org/10.2139/ssrn.4113969.
79. Mohan S, et al. Nano-structured nickel oxide based DNA biosensor for detection of visceral leishmaniasis (Kala-azar). Analyst. 2011;136(13):2845–51.
80. Iqbal A, et al. Detection of *Cryptosporidium parvum* oocysts on fresh produce using dna aptamers. PLoS ONE. 2015;10(9): e0137455.
81. Moradi M, et al. A label-free, PCR-free and signal-on electrochemical DNA biosensor for *Leishmania major* based on gold nanoleaves. Talanta. 2016;161:48–53.
82. Hao Q, et al. Electrocatalysis of thiolated single strand DNA on gold electrode for [Fe (CN)6]3-/4. Nanjing Li Gong Daxue Xuebao/J Nanjing Univ Sci Technol 2009;33:388–392.
83. Hassani S, et al. Novel label-free electrochemical aptasensor for determination of Diazinon using gold nanoparticles-modified screen-printed gold electrode. Biosens Bioelectron. 2018;120:122–8.
84. Mirzaeizadeh Z, et al. Smart early diagnosis of acute myocardial infarction: a ZIF-based nanofluorescence lateral flow immunoassay for point-of-care detection of cTnI. Mater Adv. 2024;6:839–48.

Publisher's Note